Kamper and Bekker *International Journal of Mechanical and Materials Engineering* (2017) 12:15
DOI 10.1186/s40712-017-0082-6

International Journal of Mechanical and Materials Engineering

ORIGINAL PAPER Open Access

Non-contact experimental methods to characterise the response of a hyper-elastic membrane

M. Kamper and A. Bekker*

Abstract

Background: Membranes often feature in dynamic structures. The design of such structures generally includes the evaluation of their dynamic characteristics, such as natural frequecies and mode shapes.

Methods: The quasi-statics ad dyamic responses of thin rubber sheeting were investigated through non-contact experimental techniques. The rubber sheeting was modelled as a membrane structure and the material was assumed to be hyper-elastic, isotopic and incompressible. Two hyper-elastic material models were considered, namely the Mooney-Rivlin model and the Neo-Hookean model. The natural frequencies and mode shapes of the hyprt-elastic membrane were anatically and numerically calculated by assuming small linear vibrations and an equi-bi-axial stress state in the membrane. To validate the mathematical analyses, experimental modal analysis was performed where the vibration response was measured with a laser Doppler vibrometer.

Results and conclusions: The analytical model, shows that the natural frequencies of the membrane depend on the initial stretch. Mathematical and experimental results agree well at the lower modes. However, measurement resolution is found to be a vital factor which limits the extraction of closely spaced modes due to difficulties with the accurate identification of nodal line in a purely experimental approach.

Keywords: Hyper-elasticity, Non-contact techniques, Membrane, Mooney-Rivlin, Neo-Hookean, Natural frequency, Mode shape, Digital image correlation

Background

The design of dynamic structures often includes continuous mechanical systems which require the evaluation of vibration responses (Hagedorn and DasGupta 2007). Membrane structures are examples of such continuous systems and are utilised in a variety of applications, including space, civil and bio-engineering. Jenkins and Korde (2006) and Jenkins and Leonard (1991) provide reviews of membrane literature, including practical applications and the static and dynamic analysis of membranes. Advantages of membranes such as low mass and stowed volume have renewed interest in deployable structures and their utilisation of membranes for terrestrial use. Space applications utilise membranes in radars, antennas, telescopes, solar concentrators and shields (Young et al. 2005; Salama et al. 2000). Further applications are found in robotics and biomedical prosthesis, such as artificial organs, sensors, actuators and transducers (Jenkins and Korde 2006; Goulbourne et al. 2004).

Natural frequencies and their corresponding mode shapes are fundamental to understanding the dynamic response of mechanical structures. A natural frequency is a frequency at which the system will vibrate if initially disturbed from rest and not subjected to any external loads (De Silva 2007). A mode shape describes the displacement pattern of the system when it is vibrating or excited at a natural frequency (He and Fu 2001). Natural frequencies and mode shapes are inherent properties of a system and form part of the dynamic characteristics termed modal parameters. The dynamic characterisation of mechanical structures is typically performed through modal analysis techniques.

*Correspondence: annieb@sun.ac.za
Sound and Vibration Research Group, Department of Mechanical and Mechatronic Engineering, Stellenbosch University, Stellenbosch, South Africa

A musical instrument was developed to be used in an active learning experience (Newstetter et al. 2010) to convey the concepts of natural frequencies and mode shapes to under-graduate engineering students in the instructional laboratory. The musical instrument is based on a combination of the Chladni plate (Chladni 2004) and an acoustic tonoscope (Jenny 2001). As shown in Fig. 1a, the instrument comprises rubber sheeting stretched over a circular tube, using a specially designed tensioning rig. A speaker, connected to an amplifier and signal generator, is placed under the tube. The frequency generator is set to a single frequency, and the user experiences this as an audible, single-pitched tone. When the excitation frequency is adjusted, the pitch of the audible tone changes accordingly. Salt is sprinkled on the rubber surface (Fig. 1b) and forms a distinct pattern when the rubber sheet is excited at one of its natural frequencies. The large salt particles concentrate at the nodal lines and nodal circles of the mode shapes.

The aim of the instrument was twofold: firstly, to facilitate deeper learning and to encourage student engagement by introducing abstract mathematical concepts through concrete, tactile, audible and visual experiences and, secondly, to show how the deeper engineering abstractions of experimental, analytical and numerical modal analysis can be used to obtain the natural frequencies and mode shapes of the tensioned rubber sheeting. As such, the question is whether the modal properties of a thin rubber material can be predicted through a carefully planned experimental investigation and how this compares to mathematically derived modal parameters.

As the rubber sheet is thin and two-dimensional and does not support bending moments, it was modelled as a membrane (Jenkins and Korde 2006). Because of the ability to respond elastically at large deformations, the rubber was assumed to be hyper-elastic (Gent 2012). Whereas experimental modal analysis requires the excitation of the membrane and measurements of the dynamic response, both analytical and numerical modal analyses require information on the material response of the rubber sheeting.

Hyper-elastic membrane models are presented in other applications including the behaviour of biological materials and tissues (Chagnon et al. 2015; Mihai et al. 2015; Rashid et al. 2012). Chakravarty (2013) modelled the wings of micro air vehicles as hyper-elastic membranes to investigate their modal parameters. Experimental modal analysis (EMA) was performed by Chakravarty and Albertani (2011) on a pre-stretched latex membrane to investigate the effects of added mass and damping on modal characteristics. Hyper-elastic membranes further model the dynamic response of dielectric elastomers (Chakravarty 2014; Mockensturm and Goulbourne 2004). Gonçalves et al. (2009) analysed the vibrations of a pre-stretched circular hyper-elastic membrane, both analytically and numerically. The linear and non-linear vibration of a hyper-elastic rectangular membrane was additionally investigated by Soares and Gonçalves (2014) using analytical and finite element (FE) models.

The experimental evaluation of the dynamic properties of thin structures often utilises non-contact methods

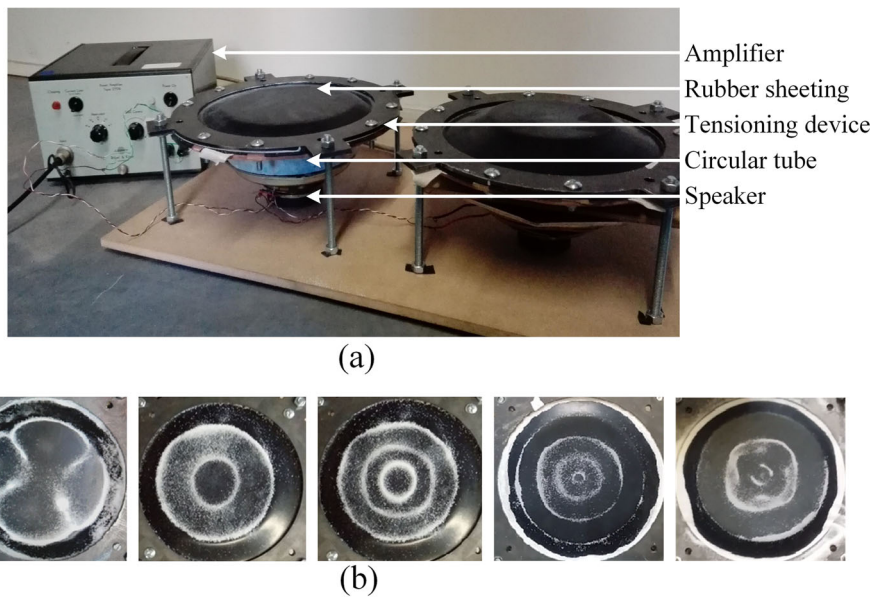

Fig. 1 a Rubber sheets are tensioned over circular tubes and excited with speakers which are placed underneath the tubes. **b** The sound frequency is varied, and the salt is used to visualise the mode shapes

(Jenkins and Korde 2006), since conventional devices, such as mechanical shakers, impact hammers and contact accelerometers, present drawbacks attributed to mass loading affects (Siringoringo and Fujino 2009). Recent studies that employ non-contact excitation and response measurement techniques (Chakravarty 2013; Siringoringo and Fujino 2009; Ameri et al. 2012; Xu and Zhu 2013) indicate that laser vibrometry is a popular tool to obtain the dynamic properties of membranes.

In light of this background, the present work documents the evaluation of experimental, analytical and numerical investigations to determine the dynamic response of a tensioned, circular, rubber membrane. To this end, hyper-elastic materials are presented first, along with the hyper-elastic material models which were considered to model rubber material. Uni-axial tensile testing was performed to determine the hyper-elastic material parameters. Digital image correlation (DIC), a non-contact technique, was used to obtain measurements of the material stretch ratio over a selected region of the rubber specimen. The natural frequencies and mode shapes of a circular hyper-elastic membrane are analytically computed by solving the two-dimensional equation of motion. The vibrations are assumed to be small, and consequently, the equation of motion in the transverse direction is linear. The analytical model is validated by experimental modal analysis. For the experimental investigation, a rubber membrane is excited through acoustic means and the response is measured with a laser Doppler vibrometer (LDV). Finally, the analytical and experimental results are compared to numerical results obtained from finite element analysis (FEA).

Methods

Constitutive modelling of rubber

Long flexible chain molecules give rise to rubber's ability to respond elastically at large deformations (Ali et al. 2010). Because of its highly elastic properties, rubber is often modelled as a hyper-elastic material. A substantial amount of literature has been published on hyper-elastic materials, including the comprehensive texts of Treloar (2005); Mooney (1940); Green and Adkins (1970) and Fu and Ogden (2001) and the collective work of Rivlin and his collaborators (Barenblatt and Joseph 1997) that contain detail on the fundamental concepts related to hyper-elastic materials. The modelling of hyper-elastic materials comprises the selection of an appropriate strain energy (or stored energy) function. For isotropic materials, experiencing homogeneous deformation, the strain energy is a function of the deformation tensor and can be expressed in terms of its invariants (Bower 2009) as

$$W = W(I_1, I_2, I_3) \tag{1}$$

where W is the strain energy and I_1, I_2 and I_3 are the strain invariants. The strain invariants are given in terms of the principle stretch ratios, denoted by λ_i as

$$I_1 = {\lambda_1}^2 + {\lambda_2}^2 + {\lambda_3}^2 \tag{2}$$

$$I_2 = {\lambda_1}^2{\lambda_2}^2 + {\lambda_2}^2{\lambda_3}^2 + {\lambda_3}^2{\lambda_1}^2 \tag{3}$$

$$I_3 = {\lambda_1}^2{\lambda_2}^2{\lambda_3}^2 \tag{4}$$

In Eq. (2) through (4), λ_1, λ_2 and λ_3 are the stretch ratios defining the amount of stretch in the principle directions. The principle stretches are defined as

$$\lambda_i = \frac{dx_i}{dX_i} (i = 1, 2, 3) \tag{5}$$

where dX_i and dx_i respectively refer to the undeformed and deformed lengths of an infinitesimal element. For an incompressible body, $I_3 = 1$. From Eq. (4),

$$\lambda_3 = \frac{1}{\lambda_1 \lambda_2} \tag{6}$$

The present work assumes that rubber responds as an isotropic, incompressible hyper-elastic material subjected to homogeneous deformation and the strain energy is therefore only a function of the first two stain invariants (Rivlin 1947).

$$W = W(I_1, I_2) \tag{7}$$

Ali et al. (2010) and Marckmann and Verron (2006) present overviews of hyper-elastic material models. The simpler models include the Neo-Hookean and Mooney-Rivlin hyper-elastic material models which were considered to represent the responses of rubber in the present work. These models require at most two material constants be determined, reducing the number of material tests (Ali et al. 2010). The strain energy function for the Mooney-Rivlin material model is defined as

$$W = C_{10}(I_1 - 3) + C_{20}(I_2 - 3) \tag{8}$$

The Neo-Hookean material model can be regarded as a simplification of the Mooney-Rivlin strain energy function and is obtained by setting C_{20} in Eq. (8) equal to zero.

$$W = C_1(I_1 - 3) \tag{9}$$

In Eqs. (8) and (9), C_1, C_{10} and C_{20} are experimentally determined material parameters. These models are limited in that they only predict the behaviour of rubber at small strains. The Mooney-Rivlin model is in good agreement for strains up to 200%, and the Neo-Hookean model approximates experimental data up to strains of 50% (Marckmann and Verron 2006). From the strain energy functions (Eqs. (8) and (9)), stress-deformation relations can be obtained for special cases of stress (Fig. 2), such as uni-axial and bi-axial stress states (Gent 2012;

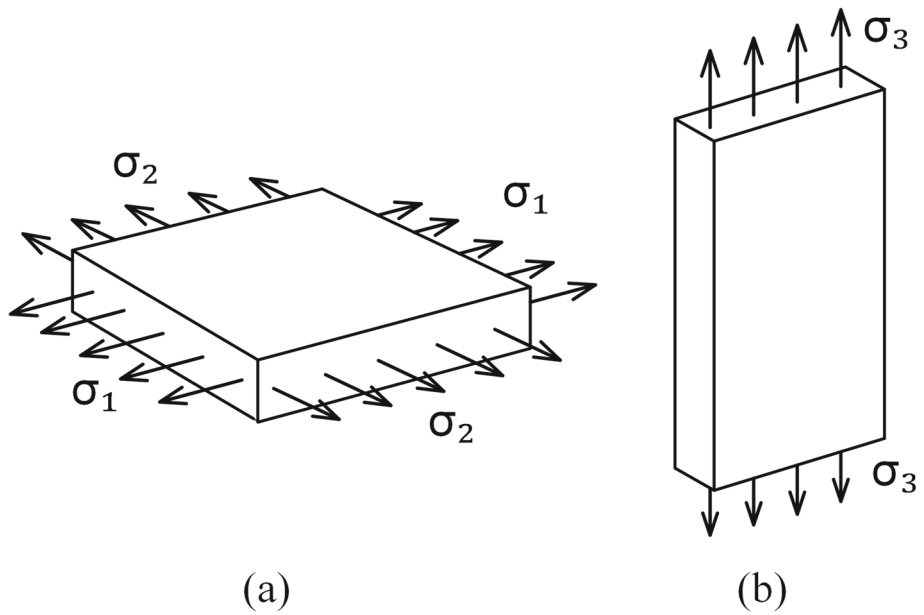

Fig. 2 Special states of stress. **a** Equi-bi-axial stress. **b** Uni-axial stress

Treloar et al. 1976). The principle Cauchy (true) stresses are expressed as

$$\sigma_i = 2\left[\lambda_i^2\left(\frac{\partial W}{\partial I_1}\right) - \left(\frac{1}{\lambda_i^2}\right)\left(\frac{\partial W}{\partial I_2}\right)\right] + p \tag{10}$$

where σ_i denotes the true stress in the three principle directions and p is an unspecified stress to prevent volume change, dependant on the state of stress. The stretch ratios, as well as the stress-deformation relationships for equi-bi-axial and uni-axial stress states are provided in Table 1.

Uni-axial material testing

Several test methods exist to determine the required hyper-elastic material parameters. These include uni-axial, bi-axial, shear and bulge tests (Kim et al. 2012; Liu et al. 2015; Sasso et al. 2008; Selvadurai 2006; Selvadurai and Shi 2012). In the present work, uni-axial tensile testing was performed on a MTS Universal Testing Machine to investigate the response of five rectangular neoprene rubber specimens (10 mm × 170 mm). The specimens were cut from 1-mm rubber sheeting with a density of 1350 kg/m^3. The same rubber sheeting was used for construction of the musical instrument. As done by Selvadurai (2006), additional pieces of rubber were glued to the grip-contact area of the rubber specimens to minimise pull out from the grips. Since the testing was performed within 30 min of applying the adhesive, the possibility of chemical reaction between the rubber specimen and adhesive can be neglected (Selvadurai and Shi 2012).

The experimental setup is illustrated in Fig. 3. The rig consisted of the MTS Universal Testing Machine and the Strain Master DIC System from LaVision. Two high-resolution cameras (Imager E-lite 2M) as well as two LED illumination units, which supplied pulsed lighting, were mounted onto a support structure. The hardware components of the DIC system (cameras, lighting, etc.) were controlled with a central control unit. Testworks software was used to control and specify the tensile test conditions, whereas the settings of the DIC system were defined with the DIC software, DaVis. DaVis was further used for image processing after the experiments were completed.

Table 1 Cauchy stress for special cases of stress states

Stress state	Stretch ratios	Neo-Hookean	Mooney-Rivlin
Equi-bi-axial	$\lambda_1 = \lambda_2 = \lambda$	$\sigma_1 = \sigma_2 = 2C_1\left(\lambda^2 - \frac{1}{\lambda^4}\right)$	$\sigma_1 = \sigma_2 = 2\left(\lambda^2 - \frac{1}{\lambda^4}\right)(C_1 + C_2\lambda^2)$
	$\lambda_3 = \frac{1}{\lambda^2}$	$\sigma_3 = 0$	$\sigma_3 = 0$
Uni-axial	$\lambda_3 = \lambda$	$\sigma_1 = \sigma_2 = 0$	$\sigma_1 = \sigma_2 = 0$
	$\lambda_1 = \lambda_2 = \frac{1}{\sqrt{\lambda}}$	$\sigma_3 = 2C_1\left(\lambda^2 - \frac{1}{\lambda}\right)$	$\sigma_3 = 2\left(\lambda - \frac{1}{\lambda^2}\right)(C_1\lambda + C_2)$

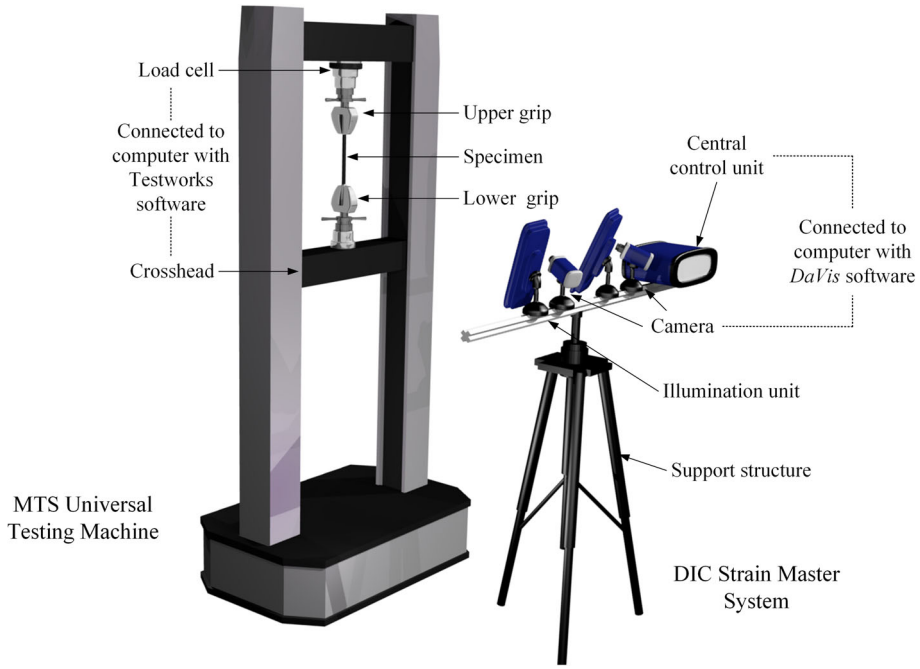

Fig. 3 Setup for tensile testing of rubber specimens consisting of the MTS Universal Testing Machine and the DIC Strain Master System

The force, measured with a 1-kN loadcell, was divided by the original cross-sectional area to obtain the engineering stress. Conventional techniques to measure the strain, such as strain gauges and extensometers, cannot be used. The rubber specimens experience large deformation during material testing, which would lead to the de-bonding or destruction of strain gauges. Two methods were considered to measure the strain. The first method was similar to that performed by Selvadurai (2006) and Selvadurai and Shi (2012). The displacement of the grips was taken to represent the change in length and the stretch ratio was calculated according to

$$\lambda = \frac{\triangle L + L_0}{L_0} \tag{11}$$

where $\triangle L$ is the change in length (i.e. displacement of the grips) and L_0 is the original length (initial distance between the grips). Homogeneous deformation is not possible over the entire section of the specimen, because

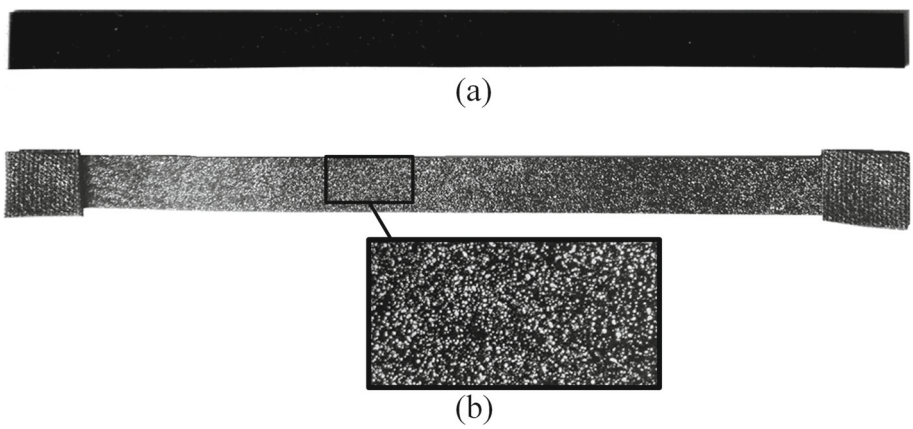

Fig. 4 a Rubber specimen without speckled pattern and **b** specimen applied with speckled pattern and additional pieces of rubber at the grip contact area

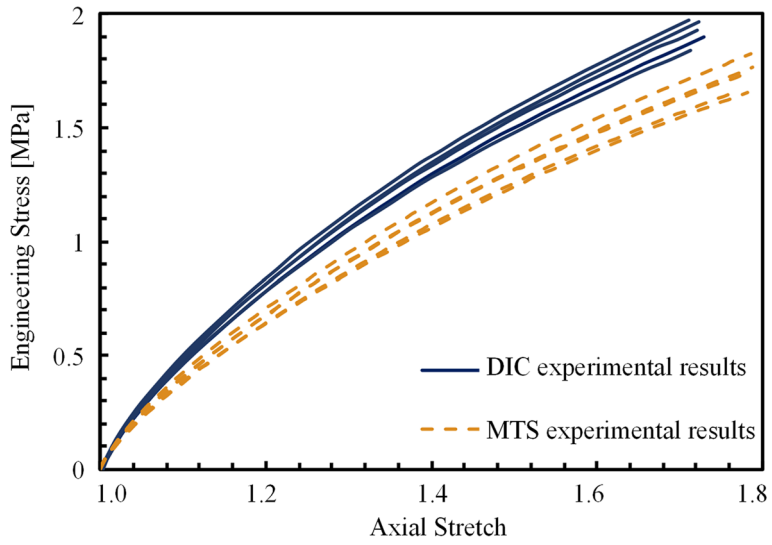

Fig. 5 Uni-axial testing results for experiments performed at a nominal strain rate of 1×10^{-3} s^{-1}

the grips prevent lateral deformation. For this reason, a second method, based on digital image correlation (DIC), was used to obtain stretch measurements over a smaller section of the specimen. The DIC optical technique tracks the movement of surface patterns on the sample to obtain information on the deformation (Pan and Li 2011). A white speckled pattern was applied to the specimens shortly before the start of each test, as shown in Fig. 4. By having the paint somewhat wet, the de-bonding of paint speckles during testing was minimised. The individual tests required roughly 20 min to complete. To achieve quasi-static conditions (and reduce the visco-elastic effects of the rubber), the specimens were tensioned at a nominal strain rate of 1×10^{-3} s^{-1}.

The experimental stress-stretch curves for both methods are reported in Fig. 5. The non-uniform deformation near the clamped area contributed to the discrepancy between the stress-stretch curves. Pullout of the specimens still occurred during testing. Hence, some displacement of the grips does not cause actual deformation of the specimen. As a result, the first method (MTS grips) overestimates the stretch ratio at a given stress. Because of the non-homogeneous deformation near the grip-area and specimen slippage, the second method is regarded as being more accurate and the material models were fit to the DIC data.

Material parameter identification

The relationship between the engineering stress and the true stress for simple loading conditions is given as

$$\sigma_{\text{eng}} = \frac{\sigma_{\text{true}}}{\lambda} \tag{12}$$

Substitution of Eq. (12) into the uni-axial stress relations (Table 1) provides the Neo-Hookean and Mooney-Rivlin uni-axial engineering stresses. The rubber is not expected to exceed a stretch ratio of 1.3 during construction or use of the musical instrument and the hyper-elastic models were fitted to each sample by matching small stretches up to 1.3. The material parameters for each hyper-elastic model, as well as the average parameter values are reported in Table 2.

To compare the Neo-Hookean and Mooney-Rivlin models, the root-mean-square (RMS) errors between the averaged experimental data and the material models were calculated. The average experimental curve as well as the two models (using the average material parameter values) are shown in Fig. 6. The RMS errors are presented in Table 3. Although the Mooney-Rivlin model provides a superior fit to the experimental data, the Neo-Hookean model was selected to describe the response of the rubber sheeting in subsequent analyses. It was reasoned that this simpler model still provides a good approximation

Table 2 Material parameters [MPa] for the Neo-Hookean and Mooney-Rivlin hyper-elastic models

	Neo-Hookean model	Mooney-Rivlin model	
Sample	C_1	C_{10}	C_{20}
1	0.797	0.140	0.806
2	0.764	0.193	0.701
3	0.825	0.152	0.829
4	0.800	0.131	0.823
5	0.768	0.142	0.767
Average	0.791	0.152	0.785

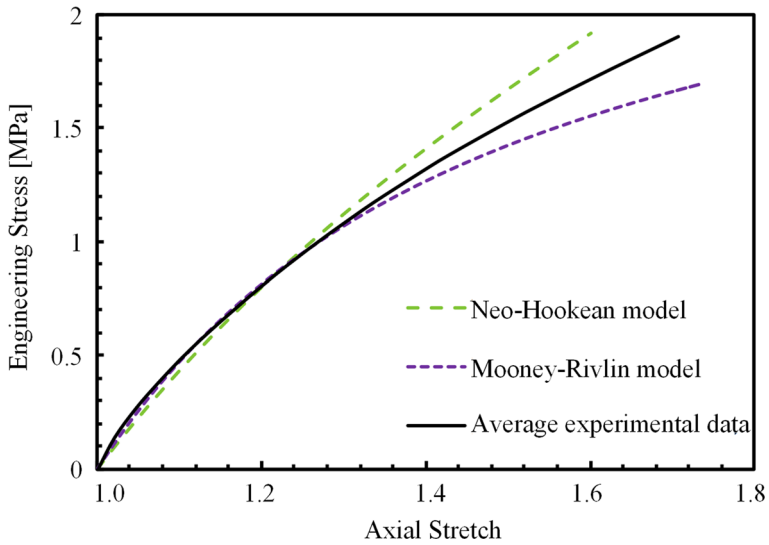

Fig. 6 Curve-fitting of hyper-elastic material models to uni-axial material testing data

in the desired strain range and is better suited to the under-graduate classroom.

Analytical analysis

To analytically obtain the natural frequencies and mode shapes of the transversely vibrating rubber sheeting, it is modelled as a flat circular membrane with an initial radius R_0. The membrane is stretched from its initial position (state 1 in Fig. 7) in the radial direction to a radius of R_f (state 2) and fixed at the boundary. The stretching of the membrane induces equi-bi-axial stresses and the Neo-Hookean material model is employed to obtain the initial stress.

This is followed by an analytical linear modal analysis about the pre-stretched state. Small vibrations (state 3) are assumed such that the equations of motion may be assumed linear. The vibration of circular membranes is a common problem in engineering applications and analytical solutions to the linear vibration of membranes are found in works such as Hagedorn, Kreyszig and Zill and Wright (Hagedorn and DasGupta 2007; Kreyszig 1999; Zill and Wright 2014). The equation of motion in the transverse direction for a vibrating membrane in cylindrical coordinates is

$$\frac{\partial^2 w}{\partial t^2} = c^2 \left(\frac{\partial^2 w}{\partial r^2} + \frac{1}{r}\frac{\partial w}{\partial r} + \frac{1}{r^2}\frac{\partial^2 w}{\partial \theta^2} \right) \tag{13}$$

Table 3 RMS errors for uni-axial material testing

Material mode	Average material constant	RMS error
Neo-Hookean	$C_1 = 0.791$ MPa	0.032 MPa
Mooney-Rivlin	$C_{10} = 0.152$ MPa $C_{20} = 0.785$ MPa	0.012 MPa

where c is the wave speed and can be expressed as

$$c^2 = \frac{\sigma}{\rho} \tag{14}$$

In Eq. (14), σ is the equi-bi-axial stress and ρ is the material density. With substitution of the equi-bi-axial stress-deformation relation, provided in Table 1, into Eq. (14), the wave speed is expressed in terms of the Neo-Hookean material parameter and the stretch ratio.

$$c^2 = \frac{2C_1}{\rho}\left(\lambda^2 - \frac{1}{\lambda^4}\right) \tag{15}$$

C_1 is the Neo-Hookean material parameter, and the stretch ratio, λ, is defined as $\lambda = R_f/R_0$. Equation (13), together with the applicable boundary condition, $w(R_f, \theta, t) = 0$, is solved to obtain the transverse displacement of the vibrating membrane, which in cylindrical coordinates is given by

$$w(r, \theta, t) = d_{nm} J_m\left(\frac{\alpha_{nm}}{R_f} r\right) \cos(m\theta) \cos(\omega_{nm} t) \tag{16}$$

where d_{nm} is the vibration amplitude, J_m is the Bessel function of the first kind order m and α_{nm} is the nth root of the Bessel function. The order of the Bessel function, m, determines the number of nodal lines, whereas n determines the number of nodal circles of the mode shape. The natural frequency of the (m, n)-mode is given by

$$\omega_{nm} = \frac{\alpha_{nm}}{R_f}\sqrt{\frac{2C_1}{\rho}\left(\lambda^2 - \frac{1}{\lambda^4}\right)} \tag{17}$$

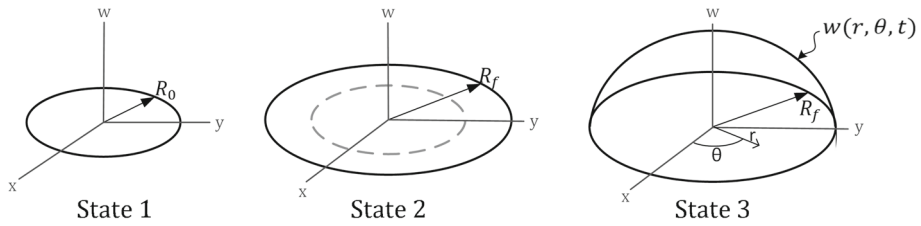

Fig. 7 Different states of deformation of a membrane

The natural frequency can also be expressed in terms of the initial radius with the substitution $R_f = \lambda R_0$.

$$\omega_{nm} = \frac{\alpha_{nm}}{R_0}\sqrt{\frac{2C_1}{\rho}\left(1-\frac{1}{\lambda^6}\right)} \tag{18}$$

Equation (18) was also obtained by Chakravarty (2013) and Gonçalves et al. (2009).

Experimental modal analysis

To validate the analytical results, experimental modal analysis (EMA) was performed to determine the modal parameters of a rubber membrane. The rubber was cut from the same 1-mm sheeting used for material testing. The material was measured to have a density of 1350 kg/m^3 and a Neo-Hookean material constant of 0.791 MPa. The rubber sheeting was stretched over a 160-mm circular tube with a simple tensioning device (Fig. 8). Two flanges secured the rubber sheeting. Holes in the flange fixture allow it to be positioned over the circular tube with threaded rods. The threaded rods were attached to a supporting back panel. To tension the rubber sheet (Fig. 8c), the flange fixture was displaced a total of 20 mm towards the back panel from the starting position (Fig. 8b).

The natural frequencies depend on the initial deformation experienced by the membrane (Eqs. (17) and (18)). Non-contact methods were employed to measure the initial stretch ratio. The flange fixture was displaced in stepwise increments towards the back panel to a final displacement of 20 mm. The membrane was subjected to bi-axial loading, and images were incrementally taken at the different stretch levels with two high-resolution cameras (Imager E-lite 2M) from the LaVision Strain Master DIC System. To obtain the in-plane stretch values, the images were again processed by the DIC software, DaVis.

A schematic layout of the experimental setup is shown in Fig. 9. The tensioned sheeting was excited acoustically with a 10-W speaker, and the response was measured with a Vibromet 500V laser Doppler vibrometer (LDV). The sound signal was amplified to ensure sufficient excitation. Classical EMA was adapted by using a free field microphone to measure the sound pressure from the speaker, which served as the reference signal. Both the microphone and the vibrometer were connected to a LMS SCADAS data acquisition (DAQ) system. Furthermore, the DAQ system provided the input signal to the speaker. Figure 10 presents the completed setup. A circular hole was cut in the back panel to allow the sound pressure waves to reach the membrane. As done by Ameri et al. (2012), the back of the panel (side facing the speaker) was covered with acoustic foam to minimise vibration of the wooden board. The sound source was placed roughly 400 mm from the tensioned rubber, and a half inch pre-polarised free field microphone was mounted to point in the direction of the source.

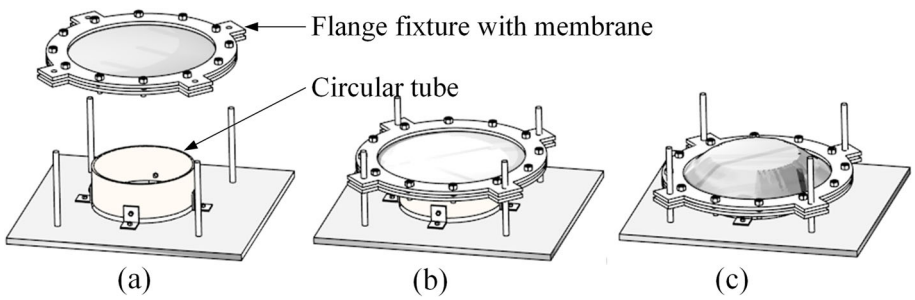

Fig. 8 Tensioning device for experimental modal analysis. **a** The membrane is held between two flanges. Threaded rods as well as a circular tube are attached two a supporting back panel. The flange fixture is used to hold the membrane at a fixed position. **b** The starting position, where the membrane barely touches the rim of the tube and does not experience any deformation. **c** The membrane is stretched over the tube by moving the flange fixture towards the back panel

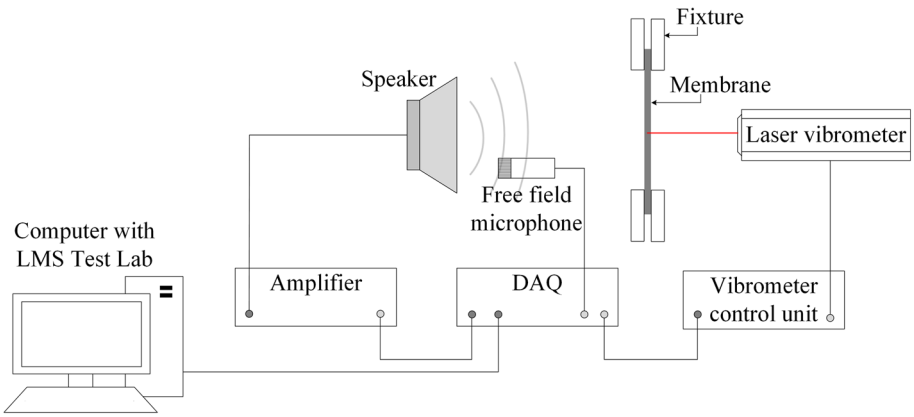

Fig. 9 Schematic layout of the hardware components for EMA

A grid pattern was drawn on the membrane with a white paint marker. The grid (Fig. 11) consisted of 41 points, arranged in a circular pattern. To identify the mode shapes, the vibrometer was moved in a roving sensor approach (Ameri et al. 2012; Xu and Zhu 2013) and measurements were captured at the 41 points of the grid. Five measurements were taken at each point and averaged to obtain the response. The frequency bandwidth was set to 1024 Hz with 2048 spectral lines and an acquisition time of 2 s for each measurement. For excitation, a linear sine sweep, spanning the bandwidth from 0 to 1024 Hz was used. The excitation and response data were processed with the LMS Test Lab software, and the modal parameters were estimated based on the Polymax algorithm.

Finite element analysis

The finite element (FE) software, Abaqus, was used to investigate the linear vibration of a pre-stretched hyperelastic membrane in order to validate the results obtained from the analytical and experimental modal analyses. A circular membrane was modelled using membrane elements with a thickness of 1 mm and a Neo-Hookean material model with a material constant of 0.791 MPa and a mass density of 1350 kg/m^3. Four-node M3D4 elements were selected to mesh the domain. (Hence, the

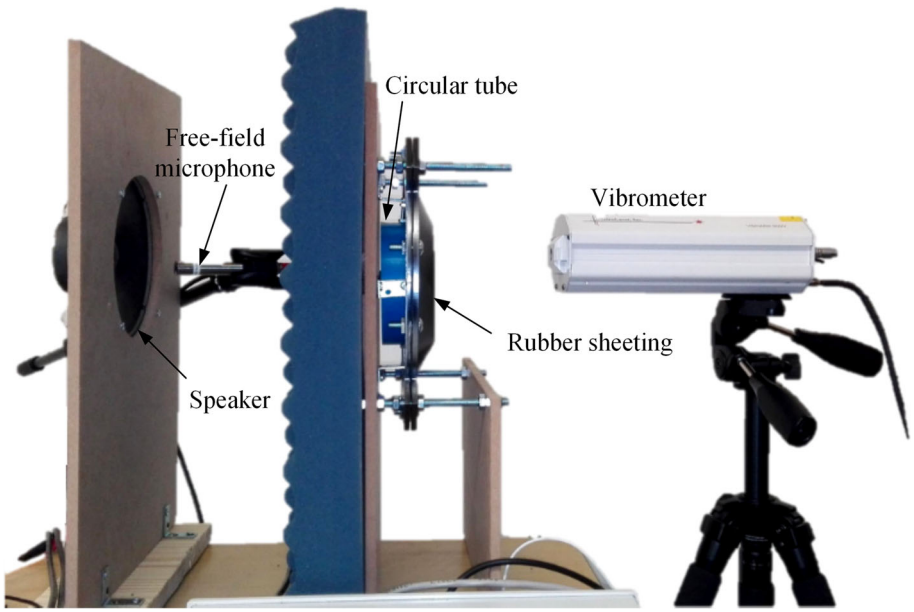

Fig. 10 EMA setup with the rubber pre-tensioned using the tensioning rig

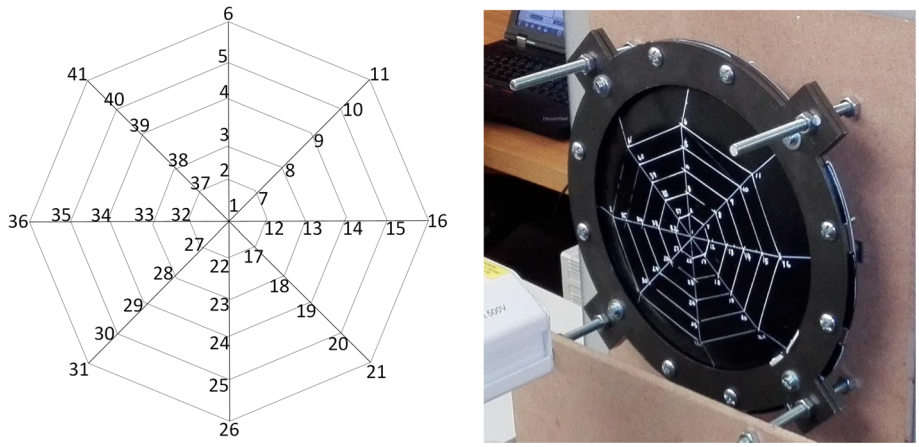

Fig. 11 Circular grid pattern and measurement points on the rubber sheeting

dominant element type was a four-node quadrilateral elements.) Some transition three-node triangular elements were allowed in order to mesh the circular domain. Similar to the analytical model, the analysis was performed in two steps. The first step consisted of a fully non-linear analysis in which a radial displacement was specified along the circumference of the membrane. To simulate the dimensions of the pipe and achieve similar conditions to that of the experimental setup, the final radius was chosen to be 80 mm. This was followed by a linear perturbation

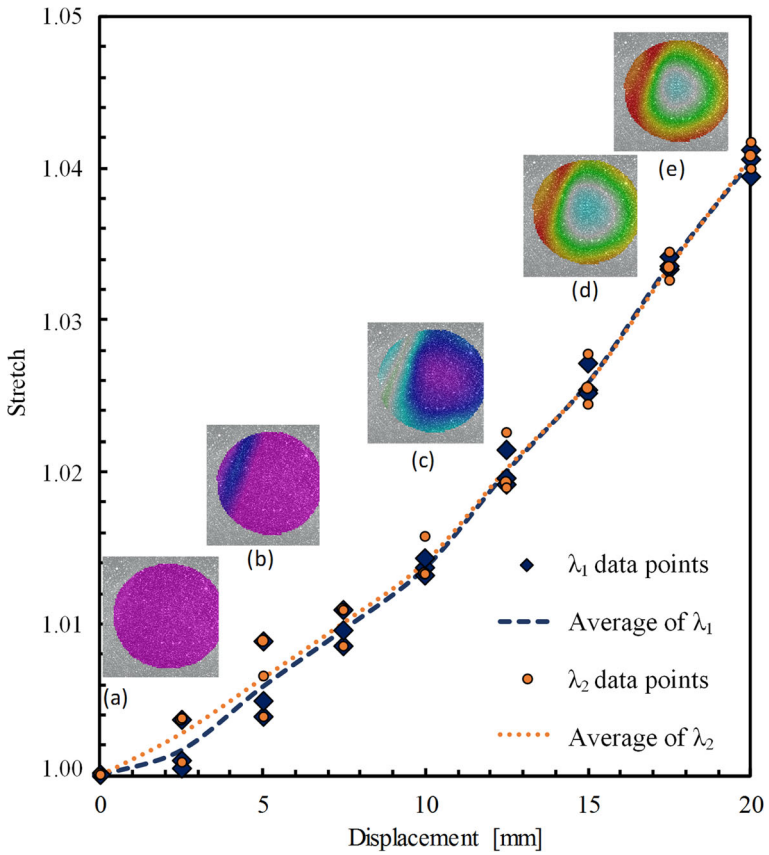

Fig. 12 In-plane stretches plotted against the displacement of the flange fixture for the rubber membrane stretched over a 160-mm pipe, together with images of the displacement field at **a** 0 mm displacement, **b** 5 mm displacement, **c** 10 mm displacement, **d** 15 mm displacement and **e** 17.5 mm displacement of the flange fixture

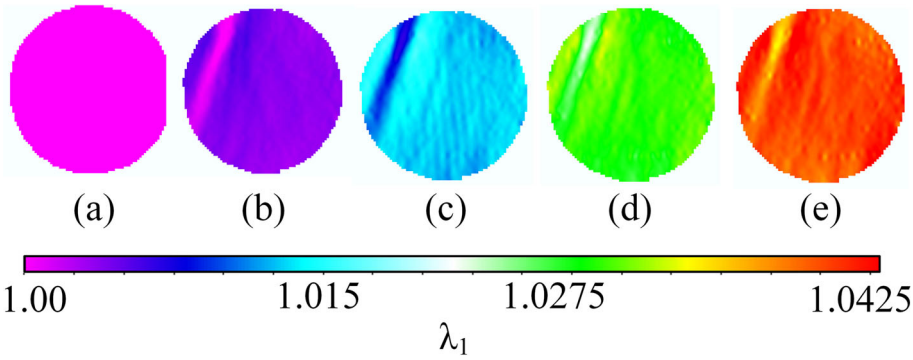

Fig. 13 Stretch field of λ_1 over the selected region at **a** 0 mm displacement, **b** 5 mm displacement, **c** 10 mm displacement, **d** 15 mm displacement and **e** 20 mm displacement of the flange fixture

step in which the natural frequencies and mode shapes were computed.

Results

Initial deformation of the rubber sheeting

Figure 12 presents the displacement of the flange fixture plotted against the computed in-plane stretches, λ_1 and λ_2, of a selected region of the membrane. It is assumed that the stretches computed for the selected region are representative of the stretches over the entire field, i.e. the stretch field is assumed to be uniform. Figure 13 presents the calculated stretch ratio, λ_1, over the surface of the selected region. The figure indicates that the stretch field is fairly homogeneous.

Also shown in Fig. 12 are inserts (a) to (e), illustrating the in-plane displacement field of the selected region with the progressive displacement of the tensioning device. The initial uneven displacement seen in inserts (b) and (c) is caused by the rubber surface not being entirely flat. As the stretch is increased, the radial displacement is increasingly more evident. At the final flange-fixture displacement of 20 mm, the in-plane stretches, λ_1 and λ_2, were respectively computed to be 1040 and 1041. Ideally, to compare the analytical and experimental results, the rubber sheeting has to be subjected to equi-bi-axial stretch. This requires the two stretch components to be equal. Even though exact equi-bi-axial stretch was not achieved, the values for λ_1 and λ_2 are still in close proximity.

Experimental modal analysis

Frequency response functions and coherence plots were generated for the velocity response measurements from the LDV and the sound pressure recorded at the microphone as shown in Figs. 14 and 15. As expected, the small speaker did not provide sufficient excitation to the membrane in the frequency range below 50 Hz, resulting in a poor coherence in this frequency range (see Fig. 15). It was found that the LDV measurements were affected by the irregularity of the rubber surface, particularly near the edge of the membrane where the surface was slightly curved. This resulted in excessive noise in the velocity response measurements in the frequency range above 350 Hz.

A stabilisation diagram, presented in Fig. 16, was calculated by LMS Polymax from the experimental modal analysis results. The Automatic Modal Parameter Selection feature was used to select poles, which correspond to the vibration modes, from the stabilisation diagram.

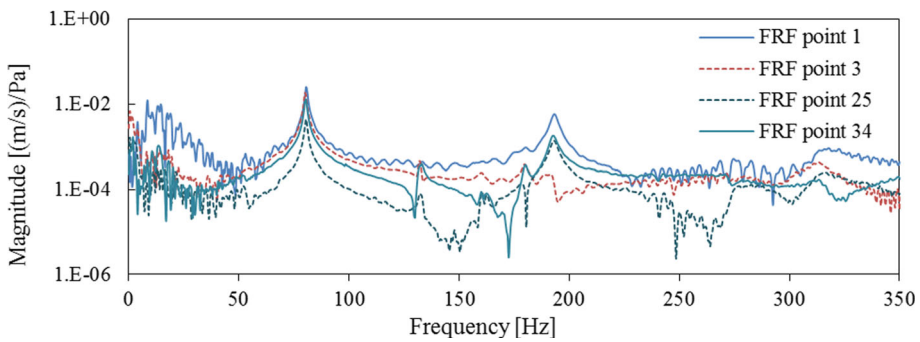

Fig. 14 Impedance FRFs for four response measurements during EMA of the membrane

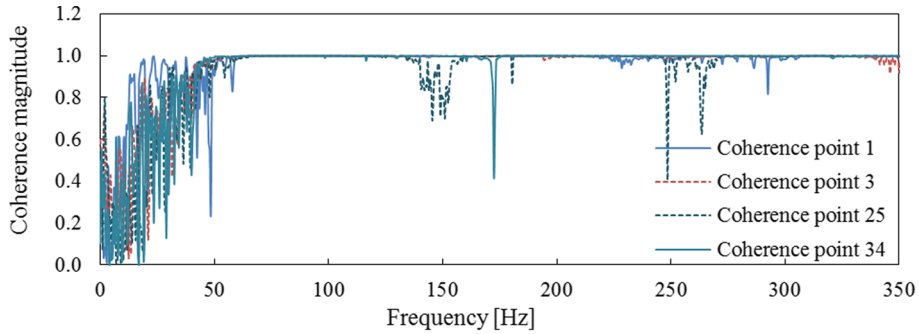

Fig. 15 Coherence plots of sound pressure and response velocity for four measurements located on the membrane

Six modes were identified in the frequency range of 50 to 350 Hz. The stabilisation diagram (Fig. 16) further presents several closely spaced modes in the frequency range between 230 and 300 Hz where no modes could be reliably extracted. The closely spaced modes are likely a results of the symmetric structure, where a given mode shape could develop at any radial location on the membrane circumference. The modal assurance criteria (MAC) (Pastor et al. 2012) matrix is reported in Fig. 17. The AutoMAC matrix presents the extent of consistency between the selected set of mode shapes.

Natural frequencies and mode shapes

To simulate similar conditions to that obtained during the experimental analysis, the circular membrane of the finite element model was specified to have an un-deformed radius of 76.9 mm. The tensioning of the membrane was simulated by specifying a displacement of 3.1 mm in the radial direction. The initial radius of 76.9 mm and radial displacement of 3.1 mm were chosen in order to achieve a similar stretch value as the experimentally computed in-plane stretches, λ_1 and λ_2. The stretched radius was therefore 80 mm with a stretch ratio of 1.0403 (R_f/R_0).

Using Eq. (17) with a stretch ratio of 1.0403 and a final radius, R_f of 80 mm, the natural frequencies can be computed analytically. The natural frequencies of five modes, determined using the different modal analysis techniques, are presented in Table 4. Since the analytically and the numerically derived frequencies are closely matched, only the percentage differences between the numerical and experimental results are provided. The percentage difference is defined as $|(\omega_n)_{EMA} - (\omega_n)_{FEM}|/(\omega_n)_{EMA}$, with

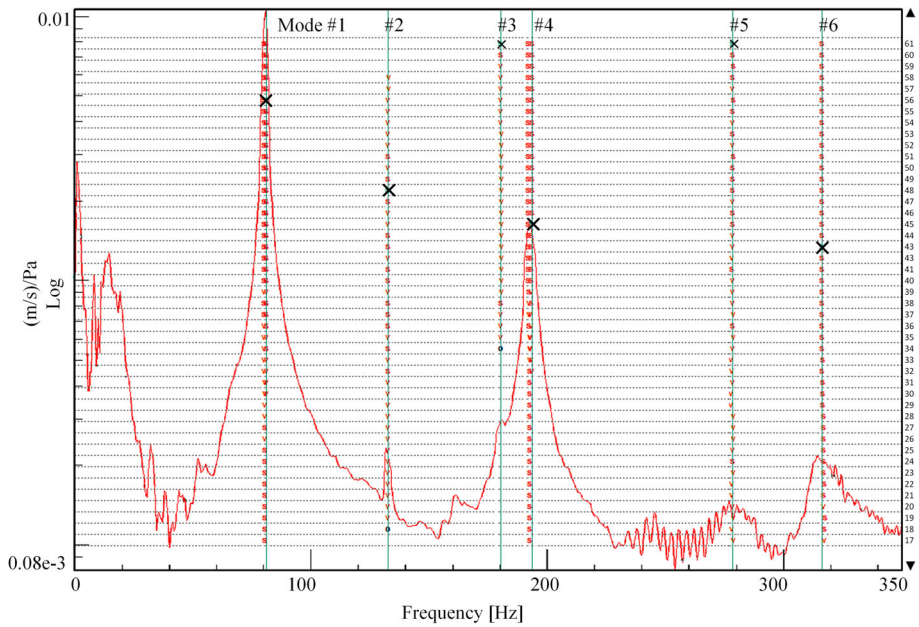

Fig. 16 EMA stabilisation diagram, showing the sum FRF with 2048 spectral lines, frequency resolution of 0.5 Hz and uniform windowing (the symbol "X" indicates selected poles)

Mode [Hz]		1	2	3	4	5	6
		80.87	132.66	180.33	193.59	278.74	316.39
1	80.87	100	3.90	9.89	21.20	2.27	4.10
2	132.66	3.90	100	2.59	5.08	3.03	2.64
3	180.33	9.89	2.59	100	14.68	0.54	0.79
4	193.59	21.20	5.08	14.68	100	18.17	14.82
5	278.74	2.27	3.03	0.54	18.17	100	65.88
6	316.39	4.10	2.64	0.79	14.82	65.88	100

Fig. 17 Tabular view of the AutoMAC matrix for EMA mode shapes

ω_n being the natural frequency. It is normalised with respect to the EMA results, as these results are based on the data collected from the actual system response. The mode shapes obtained numerically and experimentally are presented in Fig. 18.

Discussion

Non-contact techniques, such as DIC to measure strain and the use of a LDV to capture vibration responses, overcome problems associated with attachment of sensors, such as strain gauges and accelerometers. To measure the out-of-plane vibrations of the rubber sheet, the LDV had to be aligned perpendicular to the surface. It was found that the LDV measurements were affected by the irregularity of the rubber surface, in particular near the edge of the membrane where the surface was slightly curved. This resulted in somewhat noisy response measurements from the LDV.

The roving sensor approach in EMA is time-consuming but can be improved with the use of a scanning laser Doppler vibrometer (SLDV). SLVDs have automatic scanning abilities and, hence, have the capability for a higher resolution of measurement points as well as faster response measurements. Because DIC requires the application of speckle patterns and the assembly of expensive equipment, this method is also relatively time-consuming. An alternative to measuring displacement of highly elastic materials, such as rubber, is the use of long-travel contact extensometers.

Table 4 Comparison of the natural frequencies [Hz] from experimental modal analysis (EMA), finite element analysis (FEA) and analytical (AN) analysis for $\lambda = 1.0403$ and $R_f = 80$ mm

Mode	(m, n)	α_{nm}	EMA	FEA	AN	Diff [%]
1	(0, 1)	2.405	80.87	78.28	78.28	3.20
2	(1, 1)	3.832	132.66	124.73	124.72	5.98
3	(2, 1)	5.136	180.33	167.15	167.16	7.31
4	(0, 2)	5.520	193.59	179.65	179.66	7.20
6	(0, 3)	8.654	316.39	281.54	281.67	11.01

α_{nm} is the nth root of the Bessel function, m refers to the number of nodal lines and n to the number of nodal circles

The AutoMAC matrix in Fig. 17 indicates a fair amount of independency between the mode shapes. The high degree of similarity between mode pairs 5 and 6 is a result of the low resolution of the response measurement grid which was not adequate to represent the mode shape of the fifth mode (Fig. 18e). As it was not possible to determine the number of nodal lines and nodal circles of the fifth EMA mode shape, it cannot be related to the FE or analytical results, and this mode is therefore not included in Table 4.

From the analytical and FE models, several closely spaced modes were identified between the fourth and sixth EMA modes. The FE computed mode shapes of the aforementioned modes are shown in Fig. 19. These modes were not identified during EMA partly due to challenges with LDV measurements and the limited resolution of the measurement grid used for EMA. From Table 4, the mathematical and experimental results agree well at the lower modes.

Rubber is expected to exhibit viscoelastic material behaviour (Gent 2012), and its response therefore depends on the rate of deformation. Hyper-elastic material models do not account for this strain-rate sensitivity, which would be increasingly dominant at higher modes with increased rates of vibration. Uni-axial material testing was used to obtain the Neo-Hookean material parameter. However, the modal analyses were performed with the assumption of a bi-axial stress state. The hyper-elastic material model can be improved by way of bi-axial material testing. Other factors that contribute to the discrepancy between the frequency values in Table 4 are the deformation-amplitude dependency, strain-history dependency (Diercks et al. 2016) and material damping of rubber as well as the boundary conditions and the

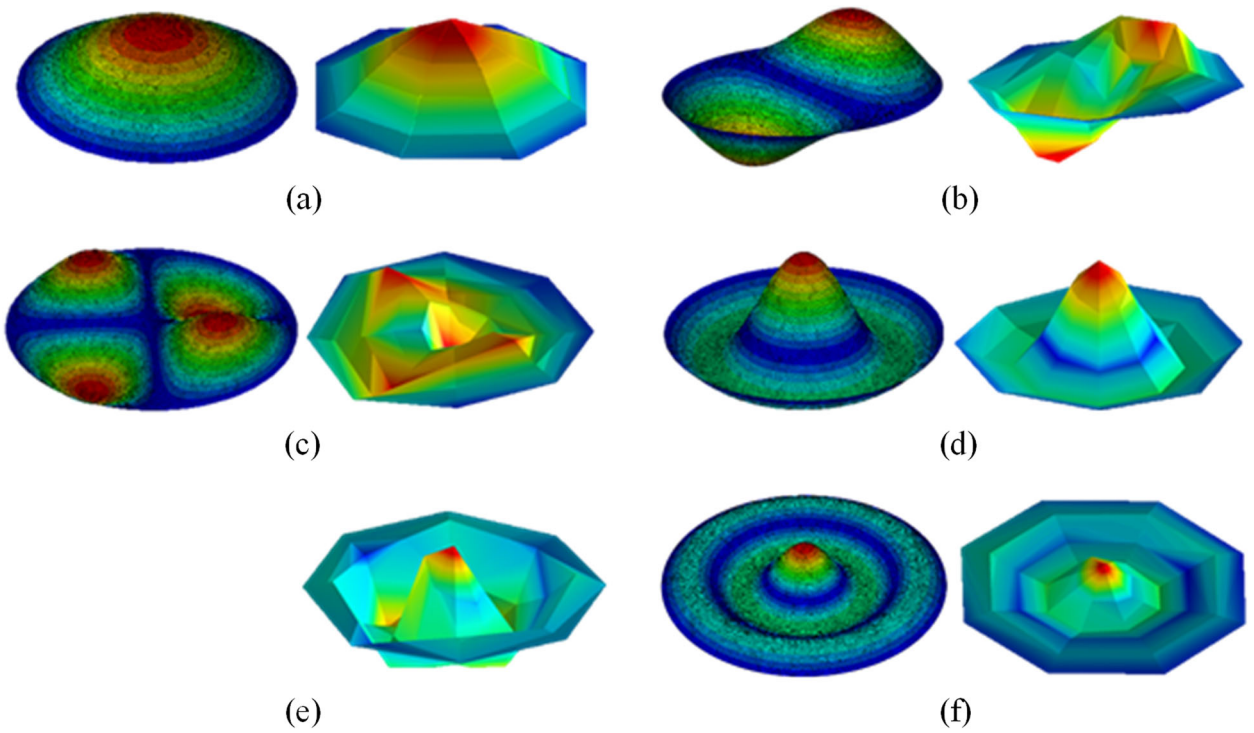

Fig. 18 Comparison of mode shapes using FEA (*left*) and EMA (*right*) for **a** mode (0,1), **b** mode (1,1), **c** mode (2,1), **d** mode (0,2), **e** not identified in FEA and **f** mode (0,3)

slippage of the sheeting between the flanges of the tensioning device. The latter results in a reduction of the actual stress experienced by the membrane. The analytical and numerical models do not account for the surrounding medium and are further limited by the assumption of small linear vibrations.

Conclusions

The analytical, numerical and experimental investigation of the natural frequencies and mode shapes of a tensioned rubber sheeting is presented. The rubber sheeting is a component of a musical instrument, which is used to explain the concepts of natural frequencies and mode shapes to under-graduate students.

The use of digital image correlation for uni-axial tensile testing was proven to be a beneficial technique in instances where slippage of test machine grips is a particular concern. For experimental modal analysis, non-contact excitation and measurement techniques were successfully employed to evaluate the modal properties of the tensioned rubber sheeting. To mathematically obtain the natural frequencies and mode shapes, the sheeting was modelled as a hyper-elastic membrane. From uni-axial material testing, it was found that the Neo-Hookean hyper-elastic model provided a good fit to material testing data for the desired strain range.

The mathematical and experimental results agree in their predictions of the natural frequency and mode

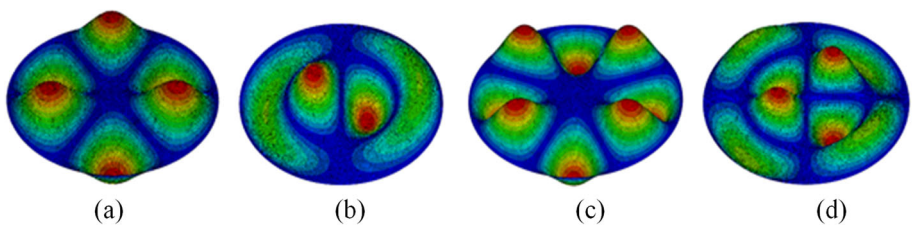

Fig. 19 Additional mode shapes that were identified with FEA: **a** mode (3,1) at 207.6 Hz, **b** mode (1,2) at 228.3 Hz, **c** mode (4,1) at 246.9 Hz and **d** mode (2,2) at 273.8 Hz

shape at the lower modes. However, some challenges are encountered with the experimental identification of closely spaced modes as a result of the limited spatial resolution of response measurements. Although spatial resolution is always a concern in EMA, this is especially applicable to symmetric circular membranes where nodal lines could be un-detected.

Discrepancies between the mathematically and experimentally derived frequencies are attributed to simplification of the complex material response exhibited by rubber, which is not completely modelled by the hyper-elastic material models. A proposed extension of the present study is the extraction of material properties from the modal test data of tensioned membranes. The modal properties of a system depend on the system's geometric and material characteristics (He and Fu 2001). Since there is good agreement between the mathematical and experimental results at the fundamental mode, it can possibly be used as a non-destructive testing method to estimate material parameters.

Authors' contributions

MK is responsible for the design of the constitutive modelling, experimental design, data acquisition and analysis presented in this work. AB initiated the project, contributed to the critical interpretation of results and experimental modal analysis and conceptualised the contribution of the manuscript, its documentation and revisions. All authors read and approved the final manuscript.

Competing interests

The authors declare that they have no competing interests.

Publisher's Note

Received: 1 July 2017 Accepted: 12 July 2017
Published online: 24 July 2017

References

Ameri, N, Tarazaga, P, di Maio, D, Ewins, DJ (2012). Non-contact operational modal analysis of an optical membrane for space application. *Topics in Modal Analysis I*, *5*, 265–275.

Ali, A, Hosseini, M, Sahari, BB (2010). Review of constitutive models for rubber-like materials. *Journal of Engineering and Applied Sciences*, *3*(1), 232–239. doi:10.3844/ajeassp.2010.232.239.

Barenblatt, GI, & Joseph, DD (Eds.) (1997). *Collected papers of R.S. Rivlin, Vols. I and II*. Berlin: Springer.

Bower, AF (2009). *Applied mechanics of solids*. Boca Raton: CRC Press.

Chladni, EFF (2004). *Die Akustik mit 12 Kupfertafeln*. Olms.

Chagnon, G, Rebouah, M, Favier, D (2015). Hyperelastic energy densities for soft biological tissues: a review. *Journal of Elasticity*, *120*, 129–160. doi:10.1007/s10659-014-9508-z.

Chakravarty, UK (2013). Analytical and finite element modal analysis of a hyperelastic membrane for micro air vehicle wings. *Journal of Vibration and Acoustics*, *135*(5). doi:10.1115/1.4024213.

Chakravarty, UK, & Albertani, R (2011). Modal analysis of a flexible membrane wing of micro air vehicles. *Journal of Aircraft*, *48*(6), 1960–1967.

Chakravarty, UK (2014). On the resonance frequencies of a membrane of a dielectric elastomer. *Mechanics Research Communications*, *55*, 72–76. doi:10.1016/j.mechrescom.2013.10.006.

De Silva, CW (2007). *Vibration: fundamentals and practice*. Boca Raton: CRC Press.

Diercks, N, Johlitz, M, Calipel, J (2016). The dynamic mullins effect: on the influence of the Mullins effect on dynamic moduli. *Proceedings of the Institution of Mechanical Engineers, Part L: Journal of Materials: Design and Applications*, *230*(3), 705–716. doi:10.1177/1464420714564712.

Fu, YB, & Ogden, RW (2001). *Nonlinear elasticity: theory and applications*. Cambridge: Cambridge University Press.

Goulbourne, NC, Frecker, MI, Mockensturm, E (2004). Electro-elastic modeling of a dielectric elastomer diaphragm for a prosthetic blood pump. *Proceedings in SPIE*, *5385*, 122–133. doi:10.1117/12.539818.

Gent, AN (2012). *Engineering with rubber: how to design rubber components*, 3rd edn. Munich: Hanser.

Gonçalves, PB, Soares, RM, Pamplona, D (2009). Nonlinear vibrations of a radially stretched circular hyperelastic membrane. *Journal of Sound and Vibration*, *327*, 231–248. doi:10.1016/j.jsv.2009.06.023.

Green, AE, & Adkins, JE (1970). *Large elastic deformations*. Oxford: Clarendon Press.

Hagedorn, P, & DasGupta, A (2007). *Vibration and waves in continuous mechanical systems*. Chichester: Wiley.

He, J, & Fu, ZF (2001). *Modal analysis*. Oxford: Butterworth-Heinemann.

Jenkins, CH, & Korde, UA (2006). Membrane vibration experiments: an historical review and recent results. *Journal of Sound and Vibration*, *295*, 602–613. doi:10.1016/j.jsv.2006.01.036.

Jenkins, CH, & Leonard, JW (1991). Nonlinear dynamic response of membranes: state of the art. *ASME Applied Mechanics*, *44*, 319–328. doi:10.1115/1.3119506.

Jenny, H (2001). *Cymatics: a study of wave phenomena and vibration*. Newmarket: Macromedia Press.

Kim, B, Lee, SB, Lee, J, Cho, S, Park, H, Park, SYSH (2012). A comparison among Neo-Hookean model, Mooney-Rivlin model and Ogden model for chloroprene. *International Journal of Precision Engineering and Manufacturing*, *13*(5), 759–764. doi:10.1007/s12541-012-0099-y.

Kreyszig, E (1999). *Advanced engineering mathematics*. Hoboken: John Wiley and Sons.

Liu, C, Cady, CM, Lovato, ML, Orler, EB (2015). Uniaxial tension of thin rubber liner sheets and hyperelastic model investigation. *Journal of Materials Science*, *50*(3), 1401–1411. doi:10.1007/s10853-014-8700-7.

Mihai, LA, Chin, L, Janmey, PA, Goriely, A (2015). A comparison of hyperelastic constitutive models applicable to brain and fat tissues. *Journal of The Royal Society Interface*, *12*(110). doi:10.1098/rsif.2015.0486.

Mockensturm, EM, & Goulbourne, N (2004). Dynamic response of dielectric elastomers. *International Journal of Non-Linear Mechanics*, *41*, 388–395. doi:10.1115/IMECE2004-61618.

Mooney, M (1940). A theory of large elastic deformation. *Journal of Applied Physics*, *11*(9), 582–592. doi:10.1063/1.1712836.

Marckmann, G, & Verron, E (2006). Comparison of hyperelastic models for rubber-like materials. *Rubber Chemistry and Technology*, *79*(5), 835–858. doi:10.5254/1.3547969.

Newstetter, WC, Behravesh, E, Nersessian, NJ, Fasse, BB (2010). Design principles for problem-driven learning laboratories in biomedical engineering education. *Annals of Biomedical Engineering*, *38*(10), 3257–3267. doi:10.1007/s10439-010-0063-x.

Pan, B, & Li, K (2011). A fast digital image correlation method for deformation measurement. *Optics and Lasers in Engineering*, *49*(7), 841–847. doi:10.1016/j.optlaseng.2011.02.023.

Pastor, M, Binda, M, Harčarik, T (2012). Modal assurance criterion. *Procedia Engineering*, *48*, 543–548. doi:10.1016/j.proeng.2012.09.551.

Rashid, B, Destrade, M, Gilchrist, MD (2012). Mechanical characterization of brain tissue in compression at dynamic strain rates. *Journal of the Mechanical Behavior of Biomedical Materials*, *10*, 23–38. doi:10.1016/j.jmbbm.2012.01.022.

Rivlin, RS (1947). Torsion of a rubber cylinder. *Journal of Applied Physics*, *18*(5), 444–449. doi:10.1063/1.1697674.

Salama, M, Lou, M, Fang, H (2000). *Deployment of inflatable space structures: a review of recent developments*. American Institute of Aeronautics and Astronautics.

Soares, MS, & Gonçalves, PB (2014). Large-amplitude nonlinear vibrations of a mooney-rivlin rectangular membrane. *Journal of Sound and Vibration*, *333*, 2920–2935. doi:10.1016/j.jsv.2014.02.007.

Siringoringo, DM, & Fujino, Y (2009). Noncontact operational modal analysis of structural members by laser Doppler vibrometer. *Computer-Aided Civil and*

Infrastructure Engineering, *24*(4), 249–265. doi:10.1111/j.1467-8667.2008.00585.x.
Sasso, M, Palmieri, G, Chiappini, G, Amodio, D (2008). Characterization of hyperelastic rubber-like materials by biaxial and uniaxial stretching tests based on optical methods. *Polymer Testing*, *27*, 995–1004. doi:10.1016/j.polymertesting.2008.09.001.
Selvadurai, APS (2006). Deflections of a rubber membrane. *Journal of the Mechanics and Physics of Solids*, *54*, 1093–1119. doi:10.1016/j.jmps.2006.01.001.
Selvadurai, APS, & Shi, M (2012). Fluid pressure loading of a hyperelastic membrane. *International Journal of Non-Linear Mechanics*, *47*, 228–239. doi:10.1016/j.ijnonlinmec.2011.05.011.
Treloar, LRG (2005). *The physics of rubber elasticity*. Oxford University Press.
Treloar, LRG, Hopkins, HG, Rivlin, RS, Ball, JM (1976). The mechanics of rubber elasticity [and discussions]. *Proceedings of the Royal Society of London A: Mathematical, Physical and Engineering Sciences*, *351*(1666), 301–330. doi:10.1098/rspa.1976.0144.
Xu, YF, & Zhu, WD (2013). Operational modal analysis of a rectangular plate using non-contact excitation and measurement. *Journal of Sound and Vibration*, *332*, 4927–4939.
Young, LG, Ramanathan, S, Hu, J, Pai, PF (2005). Numerical and experimental dynamic characteristics of thin-film membranes. *International Journal of Solids and Structures*, *42*, 3001–3025.
Zill, DG, & Wright, WS (2014). *Advanced engineering mathematics*, 5th edn. Burlington: Jones and Barlett Learning.